Time-dependent springback prediction with stress relaxation effect for non-isothermal hot stamping of titanium alloy sheets

Yuan Chen[1,2] · Guofeng Han[1,2] · Shuhui Li[1,2] · Yongfeng Li[1,2] · Zhiqiang Li[3] · Zhongqin Lin[1,2]

Abstract

The hot stamping of titanium alloy sheets is a non-isothermal forming process due to the interfacial heat transfer while hot blank is formed and cooled in cold forming tools. Due to the condition of high temperature, the material experiences a thermal-mechanical coupled deformation and a time-dependent stress relaxation subsequently. The control on shape accuracy of hot-stamped titanium alloy parts is of great challenge owing to the complicated stress evolution mechanism. The accurate prediction of springback requires a comprehensive description on the temperature and strain rate sensitive deformation, and also on the stress relaxation during die quenching. The precise testing methods and constitutive models are crucial for accurate simulation. In this work, tensile tests with different temperature and strain rates, and stress relaxation tests with different temperature and initial stress levels are performed in Gleeble system. An integrated physically based constitutive model is developed to describe both the thermo-mechanical behavior and time-dependent stress relaxation in hot stamping process. Furthermore, the proposed model is implemented in the hot stamping simulations of U-shape part through user subroutines. The essential effect of stress relaxation on stress evolutions of U-shape part is analyzed. The simulation results show promising agreement with experiments when stress relaxation is taken into account. Finally, based on the principle of increasing temperature to enhance stress relaxation, increasing the forming speed is found to be an effective way to reduce the springback of titanium alloy in hot stamping.

1 Introduction

The titanium alloy sheet components have been extensively used in aerospace industry owing to their high specific strength and good behavior in resisting creep and corrosion under extreme conditions. For example, Ti-6Al-2Mo-2V-1Zr (referred to as TA15), a near alpha titanium alloy, is a typical material used in aircrafts and aero engines in China, mostly for load-bearing components such as

landing gear, thrust reversal, and afterburner structures. Due to the poor formability at room temperature, the titanium sheet components are commonly manufactured under elevated temperatures, such as isothermal forming, superplastic forming, and creep forming, which leads to high cost, high energy consumption, and low efficiency [1]. Inspired by the manufacture method of automotive parts of boron steel, hot stamping process is found to be a promising solution to overcome these problems for titanium alloy sheet components in recent years. Zamzuri et al. [1] developed a hot stamping process for a U-shape bending of Ti-6Al-4V sheet using resistance heating and found it was effective in improving the productivity. Kopec et al. [2] investigated the hot stamping process of Ti-6Al-4V sheet and proposed a process window of temperature for forming qualified parts. Figure 1 shows the typical procedure in hot stamping process [3]. A blank is heated up and kept at elevated temperature, then transferred to cold forming tools and subsequently, formed and quenched simultaneously in tools. This process not only takes the advantage of

✉ Shuhui Li
lishuhui@sjtu.edu.cn

1   State Key Laboratory of Mechanical System and Vibration, Shanghai Jiao Tong University, Shanghai, 200240, China

2   Shanghai Key Laboratory of Digital Manufacture for Thin-walled Structures, Shanghai Jiao Tong University, Shanghai, 200240, China

3   AVIC Manufacturing Technology Institute, Beijing, 100024, China

Fig. 1 Typical process of titanium alloy sheets hot stamping
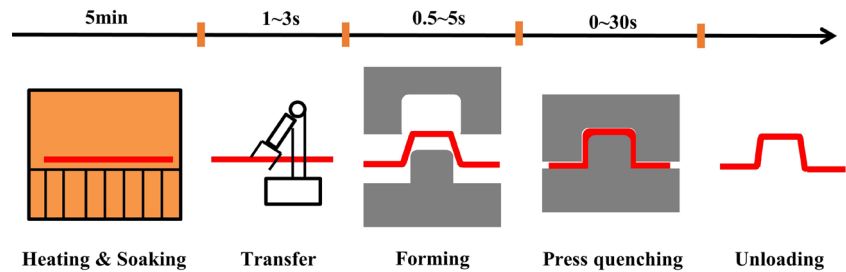
high formability at elevated temperature but also tailors the mechanical properties through die quenching, which is similar to the near-β forging process.

During forming and quenching process of hot stamping, the temperature of complex parts exhibits a non-uniform distribution and a rapid decline over time. Meanwhile, the material experiences a thermal-mechanical coupled deformation and a time-dependent stress relaxation subsequently. Due to these complicated stress evolution mechanisms, the springback of hot-stamped titanium alloy parts exhibits some special characteristics which are totally different from those of isothermally formed titanium alloy parts and hot-stamped boron steel parts. For traditional isothermal hot forming of titanium alloy sheet parts, internal stress is fully released at uniform elevated forming temperature, which results in little springback. For hot-stamped boron steel sheet parts, transformation from austenite to martensite introduces a volume expansion and a corresponding stress relaxation, which also reduces springback greatly. However, springback for hot-stamped titanium alloy sheet parts is more significant and complex. On one hand, the large deformation and internal stress in forming process have a significant effect on the stress relaxation in quenching process, which brings non-negligible influence on springback. On the other hand, different from the long-term and full stress release of isothermal forming, the stress relaxation of titanium alloy mainly happens in the first few seconds of quenching process in hot stamping. Hence, this kind of stress relaxation is short-term and insufficient. Furthermore, for die quenching of titanium alloy parts, no stress relaxation results from volume expansion in phase transformation just like that of boron steel. As a result of the issues mentioned above, the complicated stress evolution in the hot stamped titanium part makes it difficult to predict the final geometry accurately. Therefore, an accurate prediction on stress evolution for both forming and die quenching process is crucial for the final springback prediction.

For thermo-mechanical behavior of titanium alloy, many constitutive models have been proposed to describe the flow behavior of titanium alloy at elevated temperature. In the existing developments, there are two main types of constitutive models. One is empirical method, which is constructed based on empirical observations and some

mathematical functions. For example, Khan and Yu [4] and Khan et al. [5] proposed a strain rate and temperature-dependent anisotropic yield criteria based on KHL model for Ti-6Al-4V titanium alloy. Zhang et al. [6] modified the Johnson-Cook model to describe the phenomenon of the adiabatic softening at high strain rates for a near-α titanium alloy. Yang et al. [7] developed an Arrhenius-type equation to describe the temperature and strain rate–dependent flow stress of TA15 alloy. These empirical models lack of physical meaning; therefore, some detailed understanding of the physical mechanisms involved during the forming process cannot be described, especially for non-isothermal conditions in hot stamping. Another type of model to describe the constitutive behavior of titanium alloy is based on physical mechanism. For example, Fan and Yang [8] proposed a physically based unified constitutive model to predict flow stress and microstructure evolution of titanium alloy at elevated temperature by internal state variable (ISV) method, which takes several microstructure evolution mechanisms into account like solution strengthening, grain size effect, dislocation movement, and dynamic recrystallization. Babu and Lindgren [9] extended the physically founded constitutive model in Lindgren et al. [10] by considering the effects of enhanced diffusivity and globularizaiton on flow softening and stress relaxation, which was suitable for a wide range of temperature and strain rates as well as different deformation mechanisms. Wang et al. [11] modified the viscoplastic model proposed by Lin and Dean [12] to consider the effect of damage combined with microstructure evolution on the flow stress of TA15 alloy at 800°C. Normally, compared to the empirical type models, these physically based ones are capable of more accurate description under complex forming conditions. However, these works are hardly able to describe the high-temperature stress relaxation of titanium alloy in hot stamping process, which results in a poor prediction accuracy on springback of hot-stamped titanium alloy parts.

For stress relaxation behavior of titanium alloy, several experimental studies have been carried out in recent years. Zong et al. [13] experimentally investigated the springback angle of v-bending at 700°C after different holding time and found that springback almost disappeared after 10min, which was caused by internal stress relaxation.

In Zong et al. [14], the short-term stress relaxation of Ti-6Al-4V alloy with a wide range of temperature and initial stress levels was systematically studied, and it was concluded that the main mechanisms of stress relaxation were mainly controlled by dislocation climb above 650°C. In the aspect of the constitutive modeling, empirical method is adopted by many researchers. Liu et al. [15] investigated the relationship between constant-load creep and constant-strain stress relaxation of Ti6Al4V at 700°C, and found that the time-dependent creep model fitted the experiment results well. Guo et al. [16] proposed a new stress relaxation model consisting of two parts caused by stress gradient of macroscopic and microscopic respectively. By converting the stress relaxation to creep, the variation of creep strain with time at different stress levels could be described. Cui et al. [17] proposed an empirical model to predict the relationship between stress and time. However, the parameters of the proposed model could not involve the effects of temperature and initial stress levels simultaneously. Luo et al. [18] investigated the stress relaxation behavior of Ti6Al4V with different grain sizes at 660°C, and they proposed a revised model based on Maxwell exponential decay function with higher accuracy and less fitting parameters. Odenberger et al. [19] adopted the Zener-Wert-Avrami stress relaxation model to study the effect of stress relaxation in holding process on springback of an aero engine structure at 700°C. However, none of these models has considered the effect of pre-strain on stress relaxation which is inherited from the previous forming process. Meanwhile, it is important to consider the effects of temperature, initial stress levels, and pre-strain simultaneously on stress relaxation, which are main features under hot stamping conditions.

The accuracy and reliability of hot stamping process simulation depend not only on the precise constitutive models but also on accurate experimental data. For hot stamping process of titanium alloy, it is more suitable to conduct both uniaxial tensile tests and stress relaxation tests in Gleeble system, a thermo-mechanical simulator, for its precise and flexible temperature control ability. However, the temperature gradient along the tensile direction of specimen caused by resistance heating in Gleeble system results in localized deformation, which affects the accuracy of strain measurement. The default strain measurement in Gleeble system provides a point-wise average result based on the stroke or L-gauge displacement. An alternative method called digital image correlation (DIC) technology has been implemented in Gleeble system in recent years, by which precise full strain field can be obtained through non-contact measurement. The strain and the strain rate used for identification of constitutive model parameters may vary among different determination methods. Kopec et al. [2] assumed an effective strain gauge length of 25mm

for Ti6Al4V based on temperature detection by using three K-type thermocouples to calculate the average strain. But the temperature difference of this region has not been mentioned. Li et al. [20] defined the strain gauge length by a criterion of 10°C temperature difference from the midpoint of the specimen and the average strain was obtained based on DIC measurement results. Li et al. [21] proposed a strain gauge length determination method based on the change of curvature in the edge profile of the boron steel specimens, which does not suit for titanium alloy due to the large continuous temperature gradient along the tensile direction. Methods based on temperature difference lack reliable analysis on the impact of different criteria, which is crucial to obtain accurate experimental data and needs to be further investigated.

The purpose of this work is to investigate on the experimental test method for titanium alloy sheets and develop an integrated physically based constitutive model through ISV method which can describe the thermo-mechanical behavior and the time-dependent stress relaxation under hot stamping conditions. Subsequently, combined with numerical simulation, the springback of titanium alloy sheet in hot stamping process can be predicted more accurately. Finally, based on the simulations, the impact of process parameters on springback is studied and a suggestion has been made to reduce the springback in hot stamping of titanium alloy.

2 Experiments details

2.1 Material

The studied TA15 alloy sheet was produced according to GJB2505A-2008 with a thickness of 1.5mm. The main composition is listed in Table 1. The as-received initial microstructure after annealing at 800°C is shown in Fig. 2, which mainly consists of equiaxed α phase with intergranular β phase.

2.2 Experiment procedure

The hot stamping process of titanium alloy sheet mainly consists of two procedures including forming process and die quenching process. In forming process, the material mainly experiences a thermal-mechanical coupled deformation, which provides an initial stress field for the subsequent stress relaxation in first few seconds of die

Table 1 Chemical composition of TA15 alloy (wt.%)

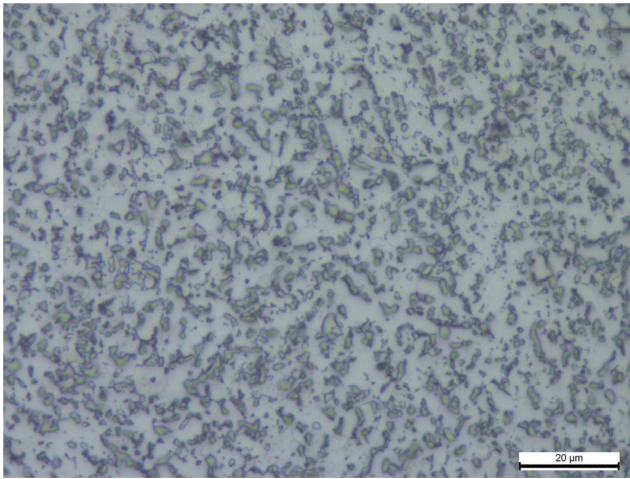| Elements	Al	V	Zr	Mo	Fe	Ti
Content	6.67	2.01	1.96	1.45	0.04	bal.

Fig. 2 The initial microstructure of TA15 alloy

quenching process. In die quenching process, the material mainly experiences thermal contraction due to cooling and stress relaxation under conditions of the initial stress and elevated temperature. The final state of stress depends on the stress evolution in above two processes, which determines the final springback. In order to reduce springback based on appropriate process parameters, it is crucial to make an accurate description of thermal-mechanical deformation and stress relaxation under hot stamping conditions. Hence, uniaxial tensile tests and stress relaxation tests of TA15 alloy are carried out in the low-load module of Gleeble3500 system to obtain the thermo-mechanical properties and time-dependent stress relaxation properties, respectively, which are essential for further parameters identification of constitutive model.

A specimen is adopted as shown in Fig. 3. The measured β-transus temperature is 995°C. For the purpose of obtaining the bi-modal microstructure which exhibits excellent comprehensive performance at elevated temperature, all specimens are heated up to 950°C (α/β phase field) and soaked for 5min as recommended by Lütjering and Williams [22].

According to the real hot stamping process, forming temperature is in the range of 650 to 850°C, and the strain rate is within 0.1–10/s. Therefore, uniaxial tensile

tests are carried out at five temperature levels which are 650, 700, 750, 800, and 850°C, respectively, as shown in Fig. 4a. Due to the non-uniform deformation caused by non-uniform temperature distribution, the strain rates are hard to determine. Therefore, within the capacity of Gleeble system, tensile speeds of 1mm/s, 10mm/s, and 50mm/s are applied to conduct tests until failure. The data of load and clamps displacement is recorded by the Gleeble system. The full field temperature and strain data are recorded by infrared temperature measure system and DIC method respectively. The measured strain data and loading forces at different temperatures and tensile speeds are converted to true stress-strain curves.

Stress relaxation tests are carried out to determine the short-term stress relaxation behavior in dependency on temperature (550, 650, 750, and 850°C) and initial stress levels (three different initial stress levels are adopted for each temperature) for 300s as shown in Fig. 4b. Loading forces are recorded and used to illustrate true stress-time curves.

2.3 Strain field measurement based on DIC method

To characterize mechanical performance of TA15 alloy during hot stamping process, it is essential to obtain precise strain data. Therefore, DIC method is applied to the present work for the accurate measurement of strain field and further strain rate calibration. A camera with max speed of 4000fps (FASTCAM MINI ux50) is utilized to record the deformation process. Meanwhile, a blue light filter and two blue light sources are used to diminish the interference of infrared light. More detail of the testing platform can be found in our previous study in Li et al. [21]. To determine the strain field distribution by DIC, a qualified speckle pattern is indispensable for hot stamping process. One notable method for the speckle pattern preparation is surface embossing as mentioned by Li et al. [21]. However, the titanium alloy exhibits a hardness up to 400HV, which makes embossing method not feasible. Hence, another method is used by covering the white boron nitride aerosol spray on the specimen surface of interest. It can be seen from Fig. 5 that the white speckle pattern works well

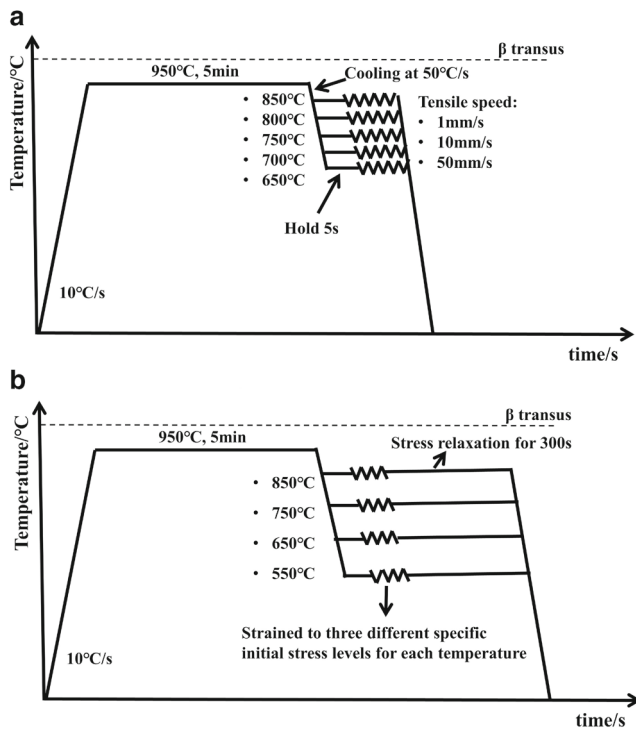**Fig. 3** Dimension of experimental specimen
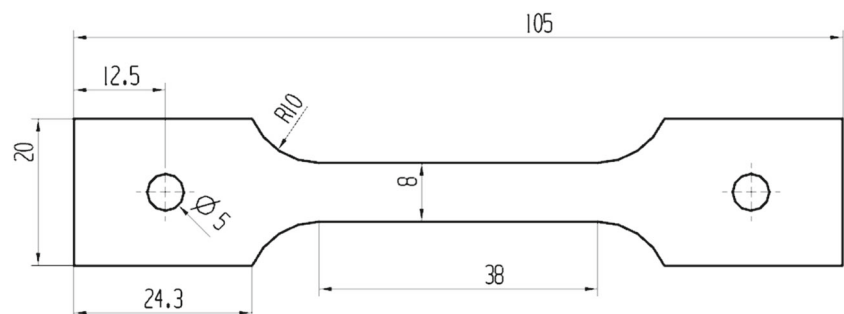
Fig. 4 Design of experiment procedures for **a** tensile tests and **b** stress relaxation tests

at 850°C with dark surface background caused by slight oxidation and keeps effective without peeling even at the strain level of 0.529. The strain field is calculated by the GOM Correlate software (GOM GmbH, Germany).

2.4 Temperature field calibration

The full field of temperature is measured by a non-contact infrared temperature measuring system for further study of different strain calculation methods which is based on the temperature distribution. The accuracy of infrared measurement is guaranteed by calibrating with the result of a platinum-rhodium thermocouples (S type) which is welded on the middle surface of the specimens for feedback
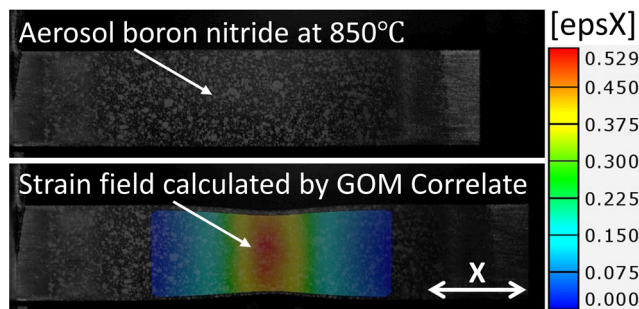

Fig. 5 Effective speckle pattern used at elevated temperature to obtain precise strain field

control on temperature during testing process. Figure 6 shows half of the temperature distribution along gauge length of TA15 alloy at different temperature levels. It is obvious that there is a large temperature gradient along gauge length direction. The temperature difference from center to the clamping end is up to 350°C. As the great temperature sensitivity for titanium alloy, it is of great significance to analyze the impact of different determination methods of uniform deformation region which is based on temperature difference on the identification of thermo-mechanical behavior, i.e., stress-strain curves.

2.5 U-shape hot stamping experiment

A U-shape forming tool is designed based on Zwick/Roell Z100 materials testing machine with a loading capacity of 100kN as shown in Fig. 7. The forming tools are made of H13 steel and painted with a layer of boron nitride as lubricant. The dimension of testing specimen is a rectangle shape with 220mm in length and 50mm in width. The punching force and the displacement are recorded by Zwick testing system. Temperature of blank is detected by a infrared thermometer assembled inside of the upper tool. Four K-type thermocouples are inserted into the specific position of the tools to measure the temperature change of tools. The procedure details of U-shape hot stamping experiment can be described as follows: Firstly, the titanium blank sheet is heated in a muffle furnace to 950°C and kept for 5min. Secondly, the heated blank is transferred from furnace to forming tools. After a response time of 1s of the machine, the upper tool starts to go down at an average speed of 10mm/s. The time for the forming and die quenching is approximately 4.5s and 30s respectively according to the video taken during the processes. The measured results, such as temperature histories of blank and
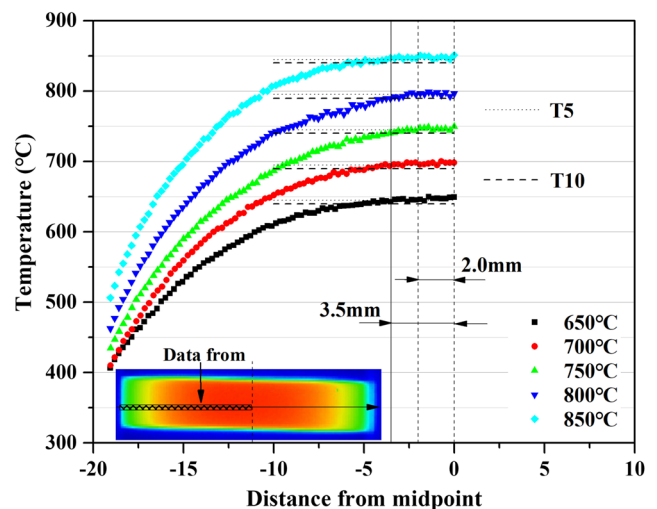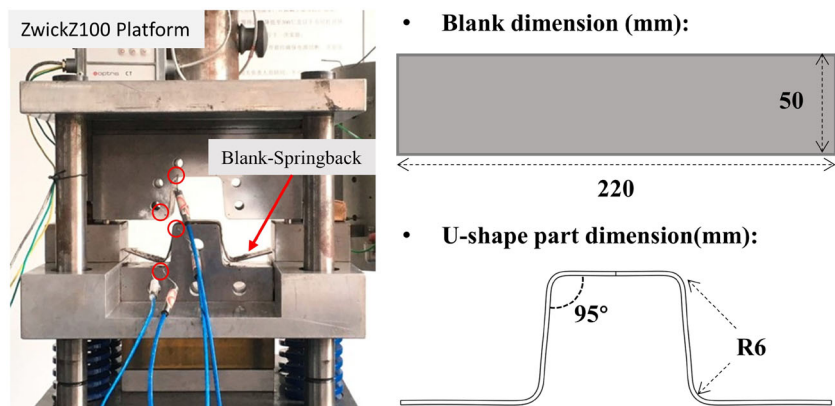

Fig. 6 Temperature distributions along the gauge length

Fig. 7 U-shape hot stamping experimental platform and dimensions of blank and part

tools with time, curve of loading force versus displacement of upper tool, and the springback of U-shape part are used to verify the the accuracy and reliability of the simulation.

3 Flow stress constitutive modeling

In this study, the constitutive model is aimed at describing the thermo-mechanical behavior and the stress relaxation behavior of titanium alloy sheets in hot stamping conditions. The dimensionless dislocation density is chosen as the internal state variable to formulate the integrated physical-based constitutive model which can link micro scale phenomena with macro scale continuum mechanics. The model mainly includes two parts: the thermal-mechanical modeling and stress relaxation modeling. For thermal-mechanical modeling, to reduce the model complexity, the mechanisms of hardening due to dislocation multiplication and softening due to dislocation annihilation, i.e., dynamic recovery, are considered. The recrystallization is not taken into account since the strain rate is high in hot stamping process as compared to the isothermal forming. For stress relaxation modeling, based on the study of Zong et al. [14], the dislocation climb is taken as the main mechanism for the short-term stress release at high temperature.

3.1 Modeling of thermal-mechanical behavior

The flow stress is assumed to include an athermal stress σ_G for long-range effect of the dislocations and a thermally activated stress σ^* for short-range effect of obstacles based on Taylor assumption:

$$\sigma = \sigma_G + \sigma^* \tag{1}$$

Derived by Seeger [23], the athermal stress part of long-range term can be expressed by:

$$\sigma_G = m\alpha Gb\sqrt{\rho_0}\sqrt{\bar{\rho}} \tag{2}$$

where m is the Taylor factor with an average value of 3, G is the shear modulus in dependency of temperature, α is a constant, and b is the Burger's vector with value of $2.95 \cdot 10^{-10}m$ [24]. The dimensionless dislocation density $\bar{\rho}$ is used to illustrate the relationship between dislocation density and the athermal stress, which is expressed as:

$$\bar{\rho} = \frac{\rho}{\rho_0} \tag{3}$$

where $\bar{\rho} \subset [1, +\infty)$ and ρ_0 is the initial dislocation density. In the undeformed material, the dislocation density is usually small. Based on calibration, Picu and Majorell [25] obtained an initial dislocation density on the order of $10^{12}m^{-2}$. Babu and Lindgren [9] used the value of ρ_0 ranging from 10^{12} to $10^{14}m^{-2}$ for a Ti-6Al-4V with annealing for 6h at 790°C. Hence, the initial dislocation density $10^{12}m^{-2}$ for TA15 alloy is used in this study.

The motion of dislocation during deformation is related to the macro plastic strain. During hot forming, plastic strain causes the multiplication of dislocation and meanwhile, softening due to dynamic recovery annihilates dislocation. Based on the model developed by Kocks and Mecking [26] which is referred to as KM model, the evolution of dislocation density with plastic strain which takes both hardening and softening effects can be expressed as:

$$\frac{d\bar{\rho}}{d\varepsilon_p} = \mu\sqrt{\bar{\rho}} - \upsilon\bar{\rho} \tag{4}$$

where μ and υ are coefficients related to the dislocation multiplication and annihilation respectively. Taking sensitivities of strain rate and temperature into account in high temperature conditions, and the athermal assumption for hardening part, μ is taken as strain rate related while υ is considered to be in dependency of strain rate and temperature, which can be expressed as:

$$\mu = \mu_0(1 - \mu_1 \ln \frac{\dot{\varepsilon}_{ref}}{\dot{\varepsilon}_p}) \tag{5}$$

$$\upsilon = \upsilon_0(1 + \upsilon_1 \ln \frac{\dot{\varepsilon}_{ref}}{\dot{\varepsilon}_p})e^{\frac{-Q_\upsilon}{RT}} \tag{6}$$

Integrating (4) gives:

$$\bar{\rho} = (\frac{\mu}{\upsilon} - \frac{\mu - \upsilon}{\upsilon} e^{-\upsilon \varepsilon_p / 2})^2 \tag{7}$$

Substituting Eqs. 7 in 1, the flow stress due to thermal-mechanical behavior can be given as:

$$\sigma = \sigma^* + m \alpha G b (\frac{\mu}{\upsilon} - \frac{\mu - \upsilon}{\upsilon} e^{-\upsilon \varepsilon_p / 2}) \tag{8}$$

The thermally activated component of stress σ^* is formulated based on an empirical function expressed as:

$$\sigma^* = K e^{-A(\dot{\varepsilon}_{ref} / \dot{\varepsilon}_p)^\delta (T/T_m)^\theta} \tag{9}$$

where K and A are material constants, and δ and θ are related to the effects of strain rate and temperature.

3.2 Modeling of stress relaxation behavior

During stress relaxation of titanium alloy, the release of internal stress associated with dislocation density can be modeled based on the Taylor equation in a square root form:

$$\sigma = m \varphi G b \sqrt{\bar{\rho}} \tag{10}$$

where m is the Taylor factor with an average value of 3, φ is a material constant, G is the shear modulus in dependency of temperature, and b is the Burger's vector. Here, $\bar{\rho}$ is the dimensionless dislocation density which is inherited from the previous deformation. Therefore, the initial stress σ_0 for stress relaxation can be expressed as:

$$\sigma_0 = m \varphi G b \sqrt{\bar{\rho}_0} \tag{11}$$

For hot stamping of titanium alloy, the stress level caused by deformation is large even in high temperature. Therefore, two driving forces of the large deformation energy and the thermal condition lead to drastic dislocation movement which annihilates the dislocations. Thus, the reduction including dislocation density results in the release of the internal stress. Based on the assumption that the dislocation climb is taken as the main mechanism for the stress relaxation at high temperature, the evolution of dislocation density can be model as:

$$\frac{d\bar{\rho}}{dt} = -\phi(\bar{\rho} - \bar{\rho}_{eq})^\gamma \tag{12}$$

where $\bar{\rho}_{eq}$ is the equilibrium value as time goes to infinity. Hence, it can be assumed that the equilibrium dislocation density is close to zero. ϕ and γ are coefficients related to the evolution rate of dislocation density which depend on both initial stress level and temperature:

$$\phi = \phi_0 e^{\frac{-Q_\phi}{RT}} \sigma_0^{m_1} \tag{13}$$

$$\gamma = \gamma_0 e^{\frac{Q_\gamma}{RT}} \sigma_0^{m_2} \tag{14}$$

Integrating (12) gives:

$$\bar{\rho} = [\bar{\rho}_0^{1-\gamma} - (1-\gamma)\phi t]^{\frac{1}{2(1-\gamma)}} \tag{15}$$

Substituting Eqs. 15 in 10, the evolution of the internal stress due to stress relaxation can be given as:

$$\sigma = \sigma_0 [1 - \frac{(1-\gamma)\phi}{\bar{\rho}_0^{1-\gamma}} t]^{\frac{1}{1-\gamma}} \tag{16}$$

where $\bar{\rho}_0$ is the initial dislocation density inherited from the previous stage. For stress relaxation tests performed in this study which are strained to three different specific initial stress levels, the initial dislocation density can be computed as:

$$\bar{\rho}_0 = \begin{cases} 1 & \text{, for elastic state} \\ (\frac{\mu}{\upsilon} - \frac{\mu - \upsilon}{\upsilon} e^{-\upsilon \varepsilon_p / 2})^2 & \text{, for plastic state} \end{cases} \tag{17}$$

Here, the initial dislocation density is related to plastic strain. Therefore, the effect of pre-strain can be also considered by Eq. 17.

Combining Eqs. 10–17 and models of thermal-mechanical behavior in Section 3.1, the integrated stress evolution of titanium alloy during hot stamping process can be described. The extended physically based KM model which includes the description of stress relaxation phenomenon can be referred to as "KM-Relaxation" model in this study. The model parameters are identified based on tensile tests and stress relaxation tests which are discussed in section of Results.

3.3 Numerical stress update of the proposed model

The numerical process for stress updating of the proposed model is illustrated in Fig. 8. The detailed calculation procedures are given below for each increment:

step 1   At the beginning of $t + \Delta t$ increment, read the variable values of stress components ${}^t \sigma_{ij}$, the equivalent stress ${}^t \bar{\sigma}$, the yield stress ${}^t \bar{\sigma}_s$, the equivalent plastic strain ${}^t \bar{\varepsilon}^p$, the dimensionless dislocation density ${}^t \bar{\rho}$, temperature ${}^{t+\Delta t} T$, increment of strain components $\Delta \varepsilon_{ij}$, and the increment of time Δt.

step 2   The stress relaxation caused by conditions such as the equivalent stress ${}^t \bar{\sigma}$, the equivalent plastic strain ${}^t \bar{\varepsilon}^p$, temperature ${}^{t+\Delta t} T$, and time is calculated based on Eq. 16. For numerical calculation, the release of stress is usually converted to creep strain which reduces the valid elastic strain. The increment of the equivalent creep strain can be expressed as:

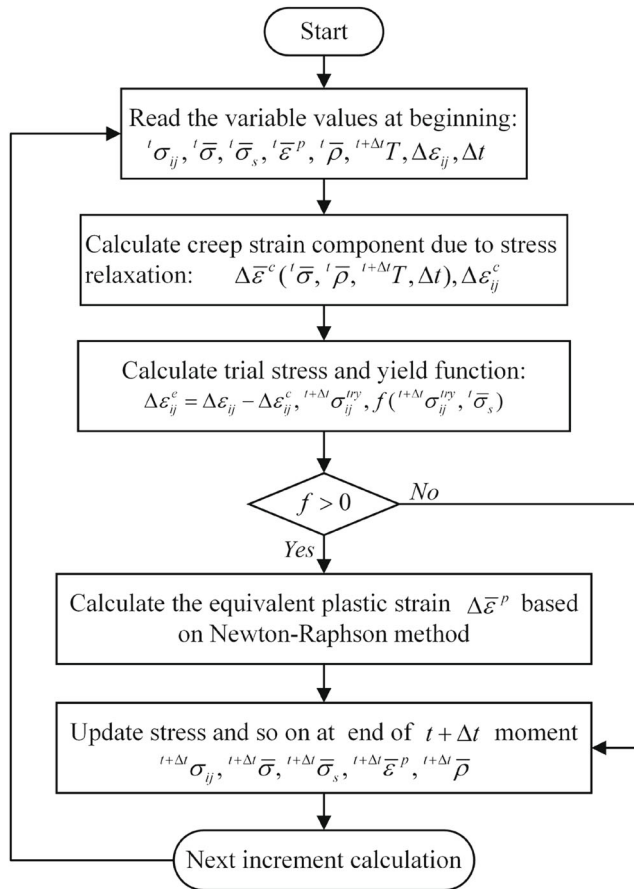$$\Delta \bar{\varepsilon}^c = \frac{-d\bar{\sigma}}{E} \tag{18}$$

Fig. 8 Numerical implementation of the proposed model for stress update

Substituting Eqs. 16 in 18 gives,

$$\Delta \bar{\varepsilon}^c = \frac{\sigma_0 \phi}{2E \bar{\rho}_0^{1-\gamma}} [1 - (1-\gamma)\frac{\phi t}{\bar{\rho}_0^{1-\gamma}}]^{\frac{2\gamma-1}{2-2\gamma}} \quad (19)$$

The increment of creep strain components can be computed based on the associated flow law.

step 3　The rest of strain increment after taking off creep strain increment is regarded as elastic for calculating the trial stress $^{t+\Delta t}\sigma_{ij}^{try}$. Then, the yield function f is computed for judging the yield state of material.

step 4　If $f < 0$, the state of material is taken as elastic and the stress can be updated directly. If $f \geqslant 0$, then the state of material is taken as elastic-plastic. Based on the associated flow law, the increment of equivalent plastic strain $\Delta\bar{\varepsilon}^p$ as well as plastic strain rate can be calculated by using Newton-Raphson iteration method.

step 5　Following the above procedures, the stress and other variables can be updated at end of $t + \Delta t$ moment and the calculation process goes into next increment.

4 Results and discussion

4.1 Comparison of different strain calculation methods

Figure 6 shows the temperature distributions from midpoint to the clamping end of the specimen. It is obvious that the temperature gradient is large for all conditions. This will result in a non-uniform deformation of the whole gauge length and cause the difficulty in calculating accurate strain rate. Therefore, the determination of strain gauge length based on temperature distribution is of great impact on the identification of constitutive parameters. Strain gauge length determination based on temperature gradient of 10°C is commonly used. To analyze the impact of temperature gradient, a harsh criterion of 5°C is chosen. Based on these two critical values, gauge lengths of 7mm and 4mm are determined as shown in Fig. 9a, which are referred to as T10 and T5 respectively.

Based on the strain gauge length determined by T10 and T5 criteria, the corresponding average strain (along gauge length) histories under condition of 850°C with 1mm/s tensile speed are recorded in Fig. 9b. It is shown that the average strain of T10 deviates greatly from the T5 after strain of 0.1. For larger deformation, the deviation becomes much more significant. It is clear that the strain rate is underestimated by T10 (0.103/s) in comparison with T5 (0.131/s). Meanwhile, the results of obtained stress-strain curves are shown in Fig. 10. Stress-strain curves of the two criteria go to different ways while downward trend for T10 and saturated trend for T5. Babu and Lindgren [9] reported that in high stacking fault material such as titanium alloy,
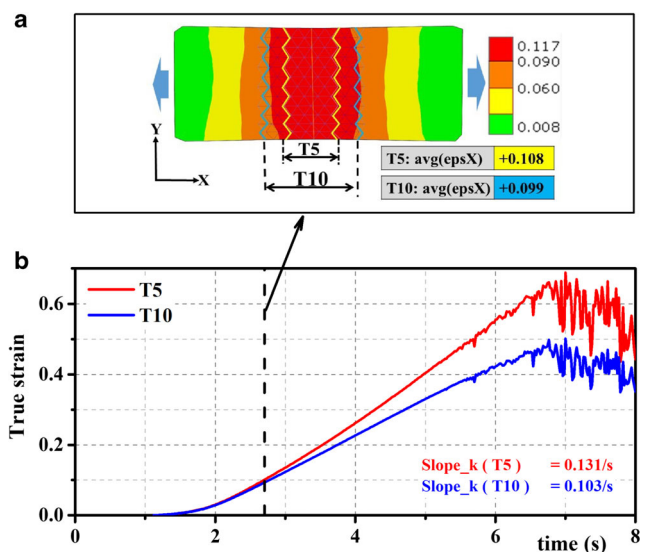

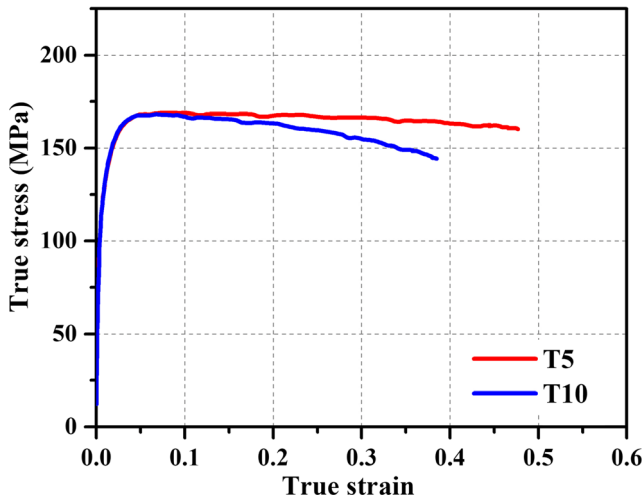**Fig. 9** Average strain **a** distribution and **b** histories at 850°C with 1mm/s tensile speed for criteria of T5 and T10

Fig. 10 The stress-strain curves obtained at 850°C with 1mm/s tensile speed for criteria of T5 and T10

Fig. 12 Stress-strain curves under different temperature

the recovery process might balance the effects of the strain hardening leading to a constant flow stress. This indicates that the results of T5 have higher accuracy due to the smaller temperature difference, while T10 may lead to wrong results for thermal-mechanical behavior. Hence, in this study, T5 criterion is adopted to obtain experimental data with higher accuracy for TA15 alloy.

4.2 Material properties and characterization

4.2.1 Thermal-mechanical behavior of TA15 alloy

The temperature-dependent elastic property of Young's modulus is shown in Fig. 11 with a linear relationship.

Figure 12 shows the temperature-dependent thermo-mechanical behavior of the material ranging from 650
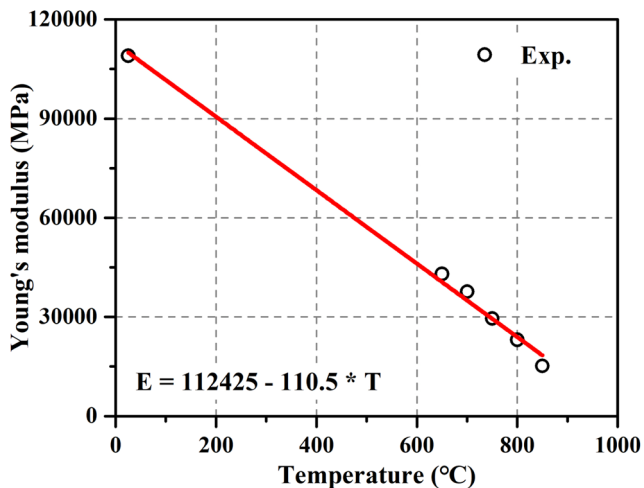
to 850°C at tensile speed of 1mm/s. Decreasing the temperature leads to an increase of flow stress and strain hardening. Moreover, with the temperature increasing, the thermo-mechanical behavior of titanium alloy tends to be ideal elastoplasticity behavior. This is mainly due to the balance of strain hardening and softening process at elevated temperature.

Figure 13 shows the dependency of flow stress on different strain rates at 750°C and 850°C. Strain rates are identified by the slope of strain histories with time in plastic range. It is clear that the flow stress of TA15 alloy is highly sensitive to strain rate. Besides, higher strain rate tests may not be performed by increasing the tensile speed which may cause the double necking phenomena. As shown in Fig. 14, the test is carried out at 750°C with tensile speed
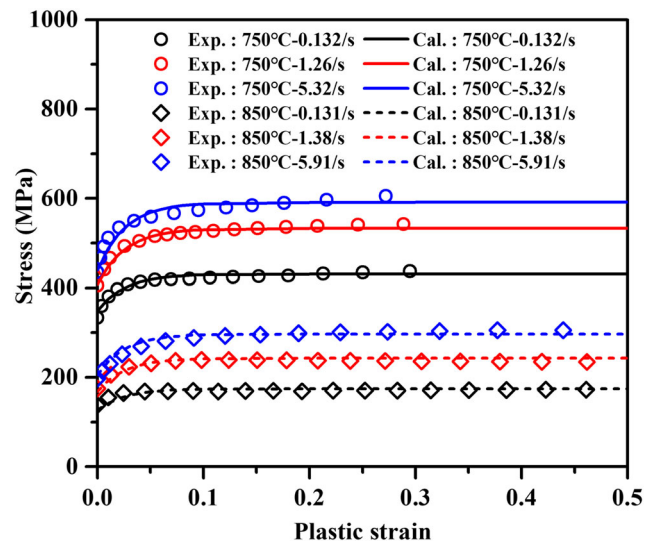

Fig. 11 The linear relationship between temperature and Young's modulus

Fig. 13 Stress-strain curves under different strain rates

Fig. 14 The strain distributions at **a** 0.01s, **b** 0.02s and **c** 0.045s under conditions of 750°C and 100mm/s
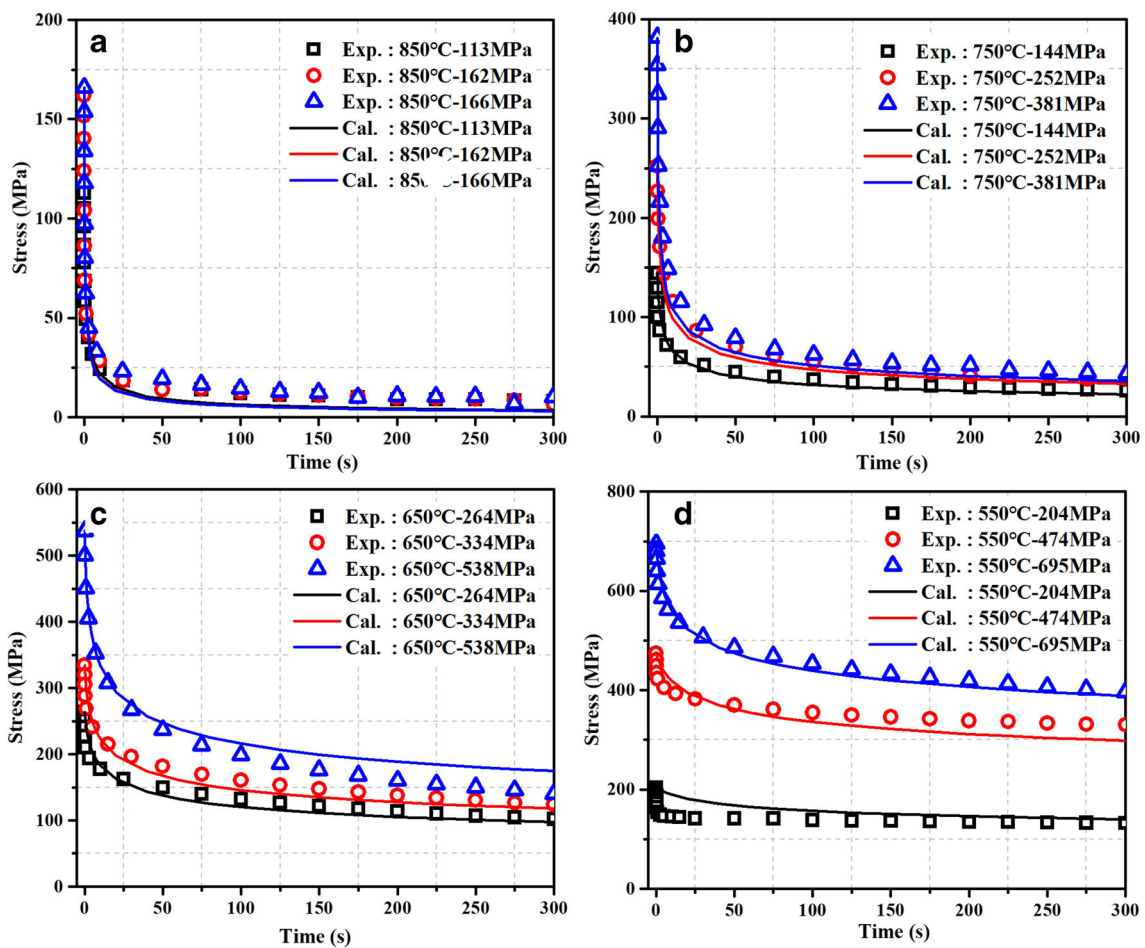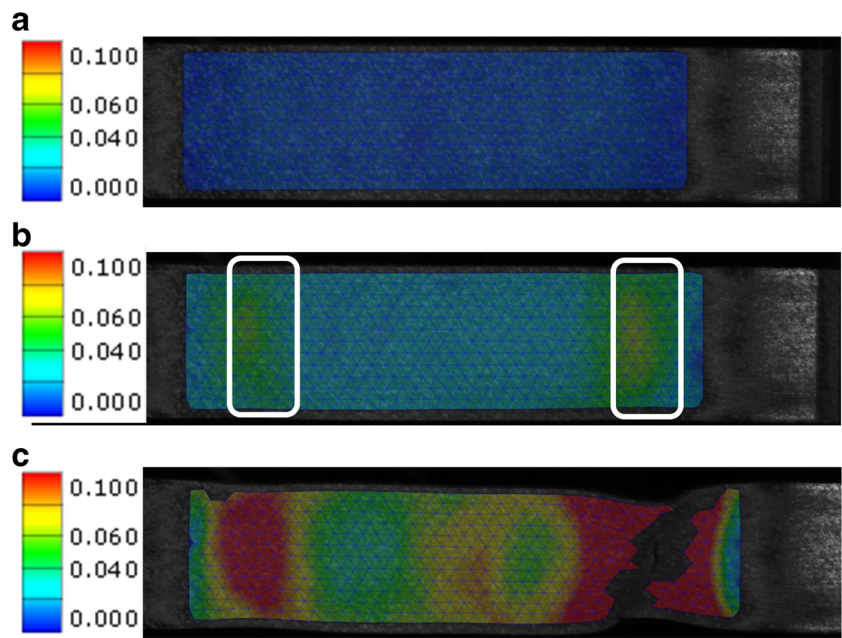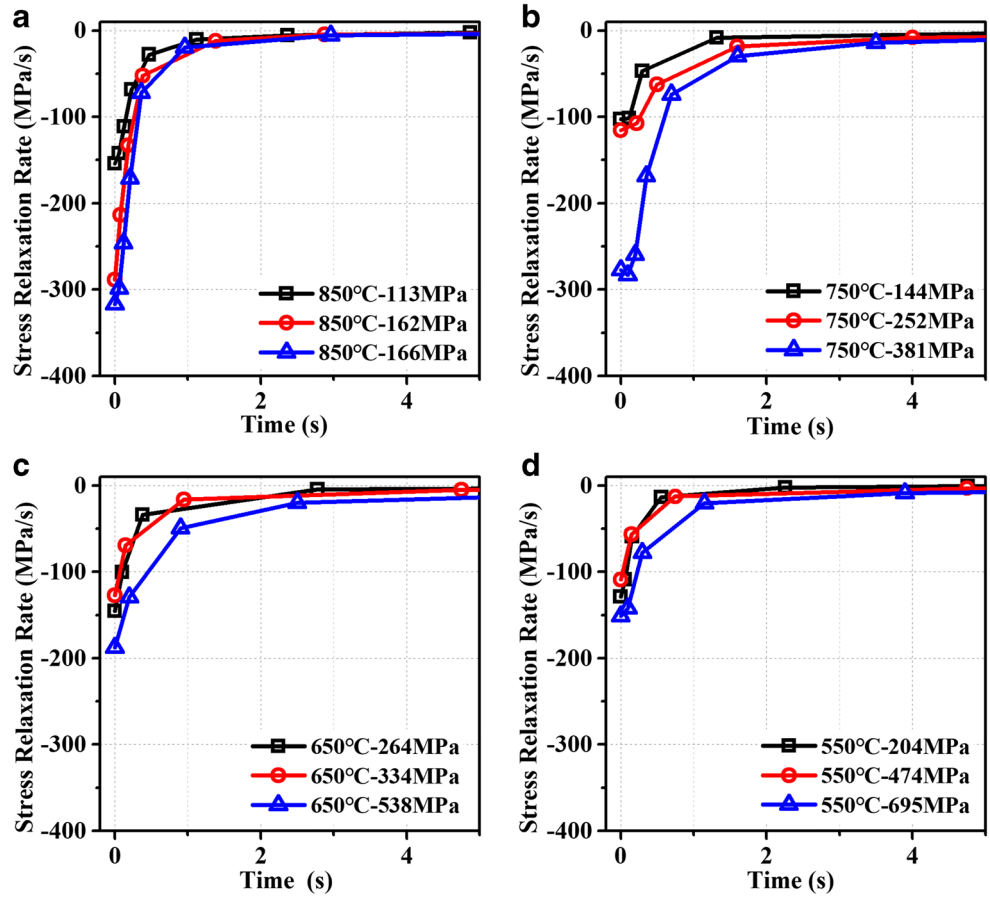

Fig. 15 Stress-time curves at temperatures of **a** 850°C, **b** 750°C, **c** 650°C, and **d** 550°C with different initial stress levels

Fig. 16 Relationship between stress relaxation rates and time at temperatures of **a** 850°C, **b** 750°C, **c** 650°C, and **d** 550°C with different initial stress levels

of 100mm/s. The frame at 0.01s shows no necking. Further deformation at frame of 0.02s leads to nearly simultaneous generation of two concentrated deformation area located equidistantly from the center. Two distinct necks, namely double necking as reported by Wood [27], are observed and one of them develops to failure at frame of 0.045s. This phenomenon has also been reported by Rusinek et al. [28] in research of steels and is attributed to wave propagation in dynamic tensile tests.

4.2.2 Time-dependent stress relaxation behavior of TA15 alloy

Time-dependent stress relaxation tests are carried out in Gleeble system with a relaxation time of 300s. The loading forces versus time at different temperature and initial stress levels are transferred to true stress-time curves as shown in Fig. 15. It is clear that stress relaxations occur strongly in the first few seconds for all conditions. Besides, stress relaxation mainly happens in the first few seconds of quenching process in hot stamping. Therefore, the first 5s of the relationship between stress relaxation rates and time are illustrated by calculating the derivative of stress-time curves as shown in Fig. 16.

These results show that both the stress and the absolute value of stress relaxation rate decrease nonlinearly as the time increases. It is obvious that the stress relaxation behavior is strongly dependent on the initial stress and
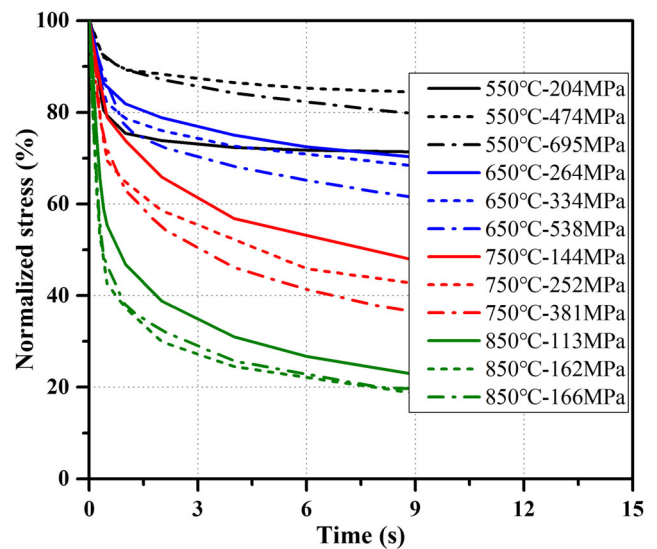

Fig. 17 Normalized stress relaxation comparison of different conditions

Table 2 The identified parameters of the proposed model

Parameters	α	$\mu_0[m^{-1}]$	μ_1	υ_0	υ_1	$Q_\upsilon[J/mol]$	$K[MPa]$	A	δ	θ
Values	0.01571	242.2	0.03386	98.90	3.071e-20	2213	376.3	286.4	0.2120	14.69
Parameters	ϕ_0	$Q_\phi[J/mol]$	m_1	γ_0	$Q_\gamma[J/mol]$	m_2				
Values	3.796e4	1.324e5	0.9272	0.1089	2.677e4	1.246e-19				

temperature. For the same temperature, with the increase of initial stress level, the absolute value of stress relaxation rate increases which could be ascribed to the higher driving force of deformation energy. This indicates that stronger stress relaxation occurs under higher initial stress level. Meanwhile, with the increase of temperature, the stress releases more sharply to low stress level which is due to high stress relaxation rate caused by higher thermal driving force.

For more intuitive understanding of the effect of temperature, normalized stress relaxations are demonstrated in Fig. 17. Here, the normalized stress is defined by the percentage of initial stress, which is expressed as $\sigma/\sigma_{initial} \times 100\%$. The stress can be released for about 80% at 850°C in the first 5s, while less than 30% can be released at 550°C. It is obvious that the stress releases more at higher temperature. Therefore, for hot stamping process, keeping temperature at a high level after forming is crucial for more sufficient stress release and reducing subsequent springback.

4.2.3 Parameter identification of the proposed model

The parameters identification of KM-Relaxation model is conducted based on global optimization algorithm by minimizing the objective function of the experi-

mental and computed values, which can be expressed as follows.

$$\delta_{error} = \sqrt{\frac{1}{N} \sum_{i=1}^{N} (\frac{\sigma_{Cal}(\varepsilon, T, \dot{\varepsilon}) - \sigma_{Exp}(\varepsilon, T, \dot{\varepsilon})}{\sigma_{Exp}(\varepsilon, T, \dot{\varepsilon})})^2} \quad (20)$$

The identification results are listed in Table 2. The calculation results of the proposed model match the experiments well within the testing conditions as shown in Figs. 12 and 13 for thermal-mechanical behavior and in Fig. 15 for stress relaxation behavior. For thermal-mechanical behavior, it is clear that the parameter of υ_1 in Eq. 6, which describes the effect of strain rate on the annihilation of dislocation density, is nearly equal to zero. This indicates that the coefficient of softening term in the model is mainly related to temperature while the hardening term relates to strain rate. For stress relaxation behavior, the index of dislocation density rate γ in Eq. 14 shows little relationship with the initial stress which is indicated by the value of m_2. From fitting results of all the tensile tests and stress relaxation tests, it can be concluded that the proposed KM-Relaxation model is competent for describing the thermal-mechanical behavior and time-dependent stress

Table 3 Thermo-physical properties of blank used in hot stamping simulation

IHTC between tools and blank		Thermal conductivity		Specific heat		Thermal expansion	
$Pressure$ (MPa)	$IHTC$ (kW/m^2K)	$Temperature$ (K)	λ (kW/mK)	$Temperature$ (K)	Cp (J/kgK)	$Temperature$ (K)	α_L (K^{-1})
0	0.337	473	9.015	373	598	373	1.398E-05
1	1.124	673	11.238	573	659	573	1.195E-05
5	2.381	873	13.877	773	698	773	1.391E-05
10	2.948	1023	15.453	973	739	973	1.585E-05
20	3.502	1123	17.361	1073	768	1073	1.781E-05
30	3.891	1223	18.198	1173	782	1173	2.257E-05

Table 4 Thermo-physical properties of tools used in hot stamping simulation

Thermal conductivity		Specific heat	
$Temperature$ (K)	λ (kW/mK)	$Temperature$ (K)	Cp (J/kgK)
298	29	298	377
373	34	373	478
473	39.4	473	510
673	44.8	673	579
873	47.5	873	735
1073	50.5	1073	821

relaxation behavior for titanium alloy under hot stamping condition.

4.3 Application of the proposed model in hot stamping process

A simulated forming process according to the hot stamping experiments in Section 2.5 is established by ABAQUS to verify the proposed model. The simulation is set to be symmetrical with X axis and Z axis. The integrated physically based model with identified parameters is applied in the ABAQUS/Explicit simulation by user subroutines of VUMAT and the simulation is referred to as "Simulation-KM-Relaxation." For comparison purpose, a simulation based on the KM model which just considers the thermal-mechanical behavior while ignoring the effect of stress relaxation is also conducted and referred to as "Simulation-KM."

Besides the material constitutive model, other details of simulation setup are declared below. A temperature drop from 950 to approximately 850°C during transfer from furnace to forming tools is detected and verified by the infrared thermometer and simulation of the transfer process considering air convection to ambient temperature of 25°C. Therefore, the initial temperature of blank is set to 850°C. The temperature of tools is set the same as room temperature of 25°C. Forming tools are regarded as rigid bodies. And the element type C3D8RT is implemented for both blank and tools.

In order to perform thermo-mechanical coupling simulation more accurately, thermal physical parameters of the material and tools are tested and listed in Tables 3 and 4, including thermal conductivity and specific heat capacity tested by laser thermal conductivity analyzer NETZSCH LFA 457, thermal expansion coefficient tested by thermal expansion instrument NETZSCH DIL 402, and the interfacial heat transfer coefficient (IHTC) between blank and tools tested by the method reported in our previous work in Li et al. [29]. A friction coefficient of 0.3 referred to the results reported by Gontarz et al. [30] is chosen at elevated temperature with lubricant condition.

The simulation results of stress distribution after die quenching are shown in Fig. 18, while (a) and (b) show the equivalent stress distribution results of Simulation-KM-Relaxation and Simulation-KM respectively. It is obvious that the equivalent stress of Simulation-KM appears to be larger than the results of Simulation-KM-Relaxation. This is due to the time-dependent stress relaxation, which leads to a reduction of final stress.

The precise prediction of stress distribution before unloading, especially through the sheet thickness, is crucial
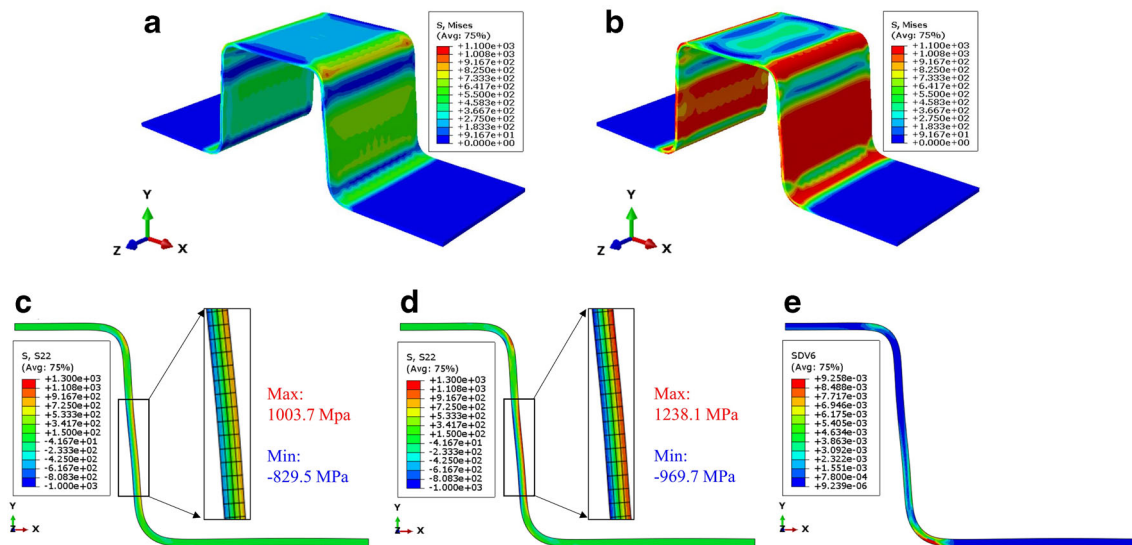

Fig. 18 Simulation results of U-shape parts: equivalent stress distributions of **a** Simulation-KM-Relaxation; **b** Simulation-KM, Stress component S22 of **c** Simulation-KM-Relaxation; **d** Simulation-KM, and **e** equivalent creep strain distribution of Simulation-KM-Relaxation
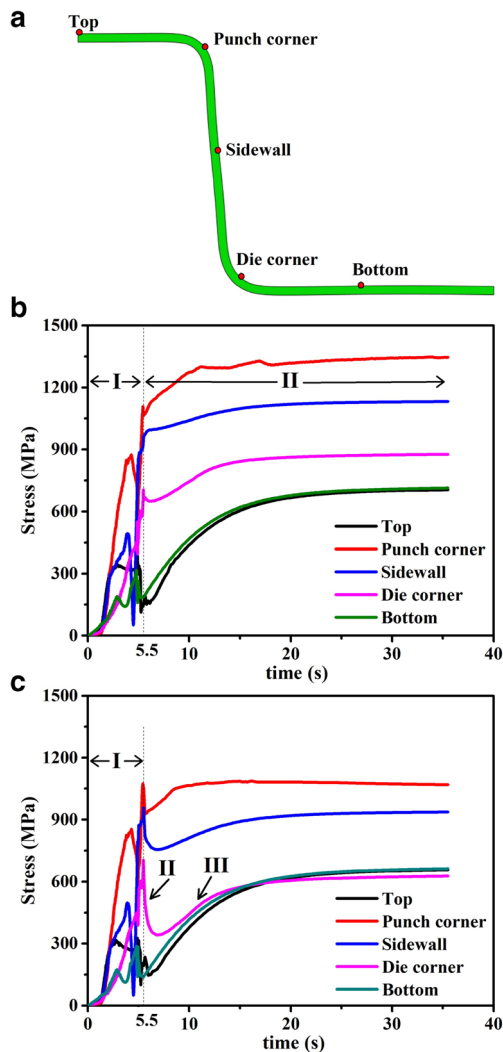
Fig. 19 History outputs of feature points: **a** the positions of feature points, **b** Stress histories of Simulation-KM, **c** stress histories of Simulation-KM-Relaxation

for the accurate springback prediction. Hence, the stress component of S22, which is along the thickness direction, is depicted in Fig. 18c and d. For the high stress regions of S22, e.g., sidewall of U-shape part, as presented in the enlarged rectangular box, the stress of outer layer is in tension state while the inner layer of stress is in compression state. This kind of stress distribution will lead to the warping of sidewall in further unloading process. The maximum and minimum stresses for the simulation results of Simulation-KM-Relaxation are 1003.7MPa and −829.5MPa respectively. When ignoring the effect of stress relaxation, the maximum and minimum stresses change to 1238.1MPa and −969.7MPa respectively. The degree of stress relaxation can be reflected by the creep strain as is shown in Fig. 18e. The maximum equivalent creep strain reached 9.258E-3 after quenching process, which occurs in the die corner.

In aspect of time, history outputs of five feature points of U-shape part are selected as shown in Fig. 19. Figure 19a shows the positions of feature points which locate in the top, punch corner, sidewall, die corner, and bottom of U-shape part. Here, $t = 5.5s$ is the time when the forming process ends. Figure 19 b and c illustrate stress histories of Simulation-KM and Simulation-KM-Relaxation respectively. It is clear that the stress histories can be divided into two stages for Simulation-KM: stage I for the forming process where stresses increase due to thermal plastic deformation and stage II for the quenching process where stresses increase caused by thermal contraction. However, considering the effect of stress relaxation, the results of Simulation-KM-Relaxation can be divided into three stages: stage I is the same as Simulation-KM and stress histories are almost the same for all feature points; stage II is different for Simulation-KM-Relaxation while stresses release quickly in the first few seconds of the quenching process; stage III begins when the temperature drops down and the thermal contraction causes the increase of stresses. Therefore, as compared with the Simulation-KM, the final stress levels of Simulation-KM-Relaxation are much lower. Furthermore, the stress histories of the top and bottom point are almost the same between the two simulations. This is because these two positions experience little stress relaxation for their low stress levels and low temperature after the forming process. However, for other positions, the stresses release in different degree in stage II due to stress relaxation. For example, the stress of die corner releases approximately 50% in stage II. It is obvious that final stresses of the Simulation-KM-Relaxation are quite different from the Simulation-KM. The accuracy of final stress state is decisive in subsequent springback prediction.

After the quenching process, springback occurs when U-shape part is unload from forming tools. The springback simulation is established by ABAQUS/Standard with implicit method. The constrained points coincide with the experimental process. The springback results of simulations and experiment are illustrated in Fig. 20. It is obvious that the shape deviation of Simulation-KM is significant, especially in the sidewall of U-shape part. Meanwhile, the result of Simulation-KM-Relaxation shows higher prediction accuracy as compared with experiments.

4.4 The influence of process parameters on springback

For industrial application, the die quenching time is an important parameter for productivity. In the case of U-shape experiment, temperature approximately drops to room temperature after 30s. Hence, to investigate the influence of quenching time (QT) on final springback of U-shape part, several simulations based on Simulation-KM-

Fig. 20 **a** Springback of experiment. **b** Comparison of springback between simulation results and experiment
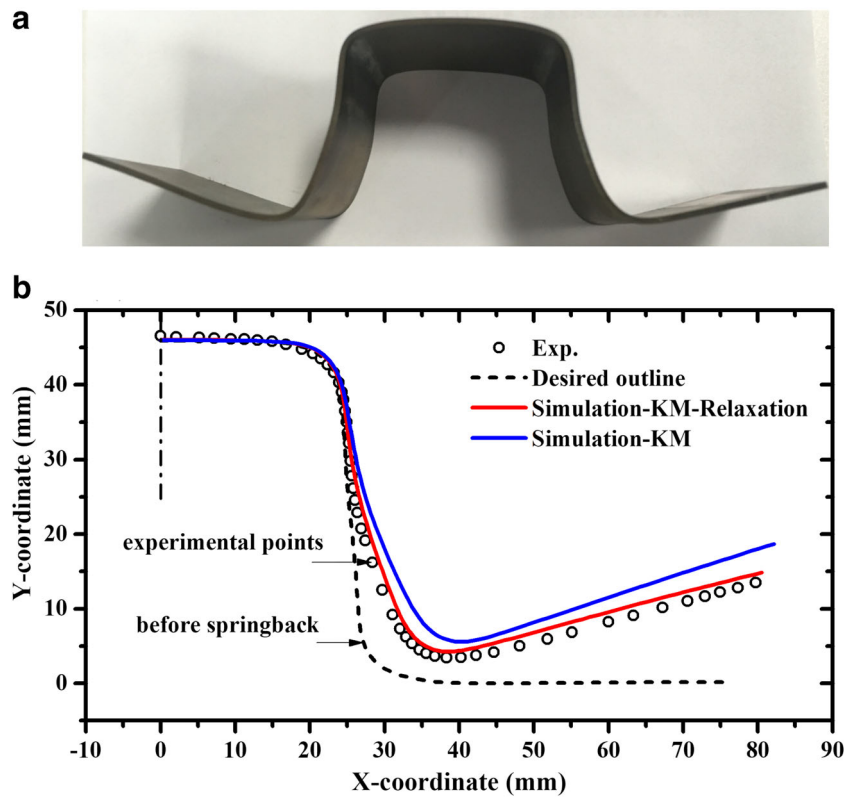
Relaxation are carried out with QT of 0s, 1s, 5s, 10s, and 20s respectively.

Figure 21 presents the springback results of different quenching time. The shape deviation is significant for the 0s of QT, which is caused by insufficient stress relaxation. However, when QT reaches 10s, the springback result is almost the same with 30s. This indicates that die quenching time can reduce to 10s for equal stress release as 30s. It can be also verified by stress histories which keep almost constant after 10s of quenching process as shown in Fig. 19c.

As analyzed in Section 4.2.2, temperature has a significant impact on stress relaxation, which is decisive in springback. Therefore, to reduce the springback, it is important to increase the temperature after forming process. For industrial applications, there are two typical strategies to increase the temperature after forming, which can be realized by increasing initial forming temperature and forming speed. Hence, based on the simulations, two initial forming temperatures (850°C and 900°C) and three forming speeds (10mm/s, 50mm/s, and 172mm/s) are chosen to analyzed their effects on springback.

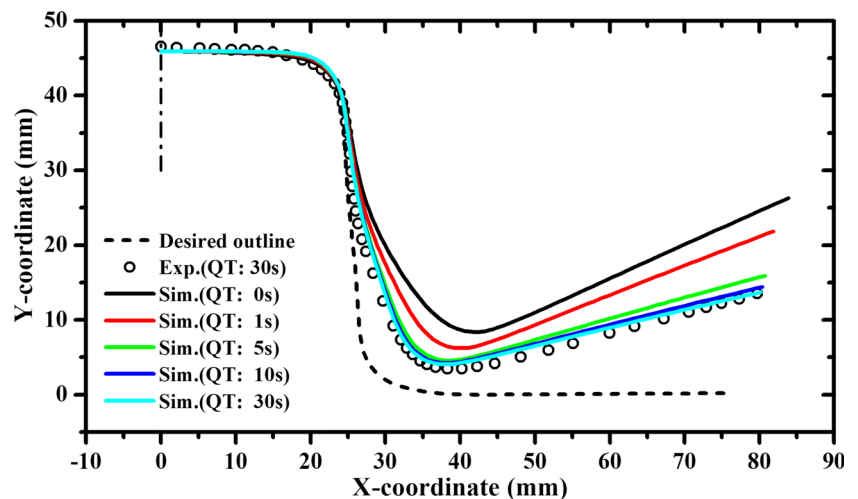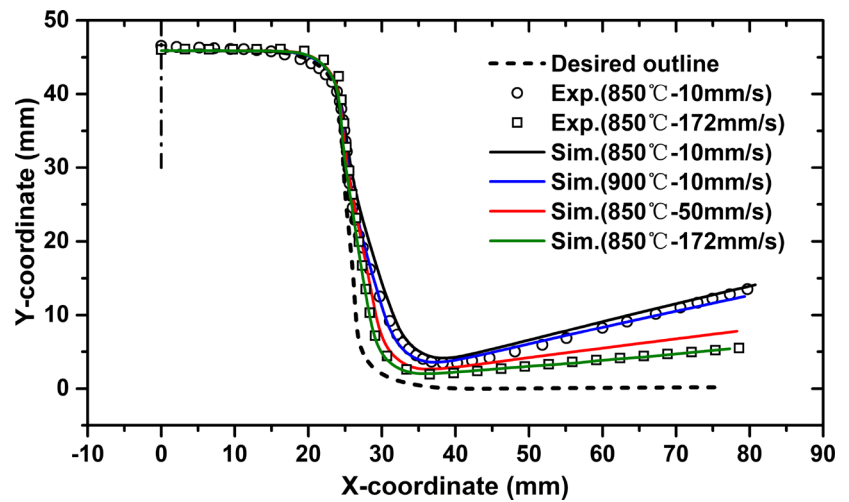**Fig. 21** The influence of quenching time on springback

Fig. 22 The simulation optimization of springback and experimental validation

The simulation results are shown in Fig. 22. It can be seen that there is little improvement for springback problem by increasing the initial forming temperature. However, it is obvious that both forming speeds of 50mm/s and 172mm/s result in a significant reduction of springback, where the forming speed of 172mm/s is validated by experiment. Therefore, it can be concluded that increasing forming speed is beneficial for the decrease of springback in hot stamping process.

5 Conclusions

The present work has investigated on testing methods, constitutive modeling, and springback prediction of a near-α titanium alloy sheet in hot stamping process. Tensile tests and stress relaxation tests are carried out using Gleeble system to study the thermo-mechanical behavior and time-dependent stress relaxation behavior in hot stamping process. Determination methods of the strain gauge length based on temperature gradient are discussed. The original physically based KM model is extended to consider the stress relaxation behavior by ISV method. Finally, the non-isothermal hot stamping simulations of U-shape part are established and verified as compared to the experimental results. Based on the simulations, the influence of process parameters on springback is analyzed. The following conclusions can be made:

(1) The determination method of strain gauge length during tensile tests has significant influence on the stress-strain curve due to the temperature gradient caused by resistance heating in Gleeble system. A harsh criterion with 5°C temperature difference is proposed to determine the uniform strain gauge length. Compared to the common practice of 10°C deviation, the obtained stress-strain curves show that 5°C deviation criterion has higher accuracy while 10°C deviation may lead to wrong results for thermo-mechanical behavior.

(2) An integrated physically based constitutive model for hot stamping of TA15 alloy is developed. Using the ISV method, this model takes underlying mechanisms of deformation and stress relaxation into account including hardening caused by dislocation multiplication, softening caused by dislocation annihilation, and stress release caused by dislocation climb. Therefore, both the thermal-mechanical behavior and stress relaxation behavior in hot stamping process can be described.

(3) By implementing the proposed model through user subroutines, simulations according to the real forming process are established. Through the comparison of springback results of simulation and experiment, the time-dependent stress relaxation is proven to be of great importance on the springback prediction accuracy in hot stamping. Meanwhile, the influence of process parameters on springback is analyzed and increasing the forming speed is found to be an effective way of reducing springback.

The proposed integrated physically based model shows promising accuracy on predicting springback. However, some shape deviation still exists as illustrated in Fig. 20. The reason may be related to anisotropic thermo-mechanical behavior of titanium alloy sheets. The hard part of this problem lies in the experimental methods of biaxial tensile tests and compression tests of titanium alloy sheets at elevated temperature. In non-isothermal hot stamping where geometry is complex in 3D dimension, it may be necessary to take this behavior into account, which is planned for future work.

Declarations

Conflict of interest The authors declare no competing interests.

References

1. Zamzuri H, Ken-Ichiro M, Tomoyoshi M, Yuya Y (2013) Hot stamping of titanium alloy sheet using resistance heating. NMSTU 5:12–15
2. Kopec M, Wang K, Politis DJ, Wang Y, Wang L, Lin J (2018) Formability and microstructure evolution mechanisms of ti6al4v alloy during a novel hot stamping process. Materials Science and Engineering: A 719:72–81
3. Karbasian H, Tekkaya AE (2010) A review on hot stamping. J Mater Process Technol 210(15):2103–2118
4. Khan AS, Yu S (2012) Deformation induced anisotropic responses of Ti–6al–4V alloy. Part I: experiments. Int J Plast 38:1–13
5. Khan AS, Yu S, Liu H (2012) Deformation induced anisotropic responses of Ti–6Al–4V alloy part II: a strain rate and temperature dependent anisotropic yield criterion. Int J Plast 38:14–26
6. Zhang J, Wang Y, Zan X, Wang Y (2015) The constitutive responses of Ti-6.6 Al-3.3 Mo-1.8 Zr-0.29 Si alloy at high strain rates and elevated temperatures. J Alloys Compd 647:97–104
7. Yang L, Wang B, Liu G, Zhao H, Zhou J (2015) Hot tensile behavior and self-consistent constitutive modeling of TA15 titanium alloy sheets. J Mater Eng Perform 24(12):4647–4655
8. Fan X, Yang H (2011) Internal-state-variable based self-consistent constitutive modeling for hot working of two-phase titanium alloys coupling microstructure evolution. Int J Plast 27(11):1833–1852
9. Babu B, Lindgren LE (2013) Dislocation density based model for plastic deformation and globularization of Ti-6Al-4V. Int J Plast 50:94–108
10. Lindgren LE, Domkin K, Hansson S (2008) Dislocations, vacancies and solute diffusion in physical based plasticity model for AISI 316L. Mech Mater 40(11):907–919
11. Wang K, Liu G, Zhao J, Huang K, Wang L (2018) Experimental and modelling study of an approach to enhance gas bulging formability of TA15 titanium alloy tube based on dynamic recrystallization. J Mater Process Technol 259:387–396
12. Lin J, Dean T (2005) Modelling of microstructure evolution in hot forming using unified constitutive equations. J Mater Process Technol 167(2-3):354–362
13. Zong Y, Liu P, Guo B, Shan D (2015) Springback evaluation in hot v-bending of Ti-6Al-4V alloy sheets. The International Journal of Advanced Manufacturing Technology 76(1-4):577–585
14. Zong Y, Liu P, Guo B, Shan D (2015) Investigation on high temperature short-term creep and stress relaxation of titanium alloy. Materials Science and Engineering: A 620:172–180
15. Liu P, Zong Y, Shan D, Guo B (2015) Relationship between constant-load creep, decreasing-load creep and stress relaxation of titanium alloy. Materials Science and Engineering: A 638:106–113
16. Guo J, Li F, Zheng X, Shi H, Meng W (2016) An accelerated method for creep prediction from short term stress relaxation tests. J Press Vessel Technol 138(3)
17. Cui X, Wu X, Wan M, Ma B, Zhang Y (2019) A novel constitutive model for stress relaxation of Ti-6Al-4V alloy sheet. International Journal of Mechanical Sciences 161:105,034
18. Luo J, Xiong W, Li X, Chen J (2019) Investigation on high-temperature stress relaxation behavior of Ti-6Al-4V sheet. Materials Science and Engineering: A 743:755–763
19. Odenberger EL, Pederson R, Oldenburg M (2019) Finite element modeling and validation of springback and stress relaxation in the thermo-mechanical forming of thin Ti-6Al-4V sheets. The International Journal of Advanced Manufacturing Technology 104(9-12):3439–3455
20. Li N, Shao ZT, Lin JG, Dean TA (2016) Investigation of uniaxial tensile properties of AA6082 under HFQ® conditions. In: Key engineering materials, trans tech publ, vol 716, pp 337–344
21. Li Y, Li S, Chen Y, Han G (2019) Constitutive parameters identification based on DIC assisted thermo-mechanical tensile test for hot stamping of boron steel. J Mater Process Technol 271:429–443
22. Lütjering G, Williams JC (2007) Titanium, 2nd edn. Springer Science & Business Media, Berlin
23. Seeger A (1956) The mechanism of glide and work-hardening in fcc and hcp metal. dislocations and mechanical properties of crystal. Wiley, Lake Placid, pp 243–329
24. Frost HJ, Ashby MF (1982) Deformation mechanism maps: the plasticity and creep of metals and ceramics. Pergamon Press
25. Picu R, Majorell A (2002) Mechanical behavior of Ti–6Al–4V at high and moderate temperatures—part II: constitutive modeling. Materials Science and Engineering: A 326(2):306–316
26. Kocks U, Mecking H (2003) Physics and phenomenology of strain hardening: the fcc case. Progress in Materials Science 48(3):171–273
27. Wood W (1967) Experimental mechanics at velocity extremes—very high strain rates. Exp Mech 7(10):441–446
28. Rusinek A, Zaera R, Klepaczko JR, Cheriguene R (2005) Analysis of inertia and scale effects on dynamic neck formation during tension of sheet steel. Acta Mater 53(20):5387–5400
29. Li Y, Li S, He J, Chen Y, Yue L (2019) Identification methods on blank-die interfacial heat transfer coefficient in press hardening. Applied Thermal Engineering 152:865–877
30. Gontarz A, Dziubińska A, Okoń Ł (2011) Determination of friction coefficients at elevated temperatures for some Al, Mg and Ti alloys. Archives of Metallurgy and Materials